REFERENCES

[1] E. H. LEE, *Viscoelastic Stress Analysis*, Proc. First Symp. Naval Struct. Mech. (Pergamon, New York 1960), p. 456.
[2] S. BREUER and E. T. ONAT, *On Uniqueness in Linear Viscoelasticity*, Quart. Appl. Math. *19*, 355–359 (1962).
[3] M. LOÈVE, *Probability Theory* (Van Nostrand, New York 1955), p. 207.
[4] N. WIENER and E. HOPF, *Über eine Klasse singulärer Integralgleichungen*, Sitzungsber. Preuss. Akad. Wiss., Phys.-Math. Klasse, Berlin (1931), p. 696.
[5] A. J. STAVERMAN and F. SCHWARZL, *Thermodynamics of Viscoelastic Behavior*, Proc. Konink. Nederlands Akad. van Wettenschappen, series B, *55*, 474–485 (1952).
[6] D. BLAND, *Theory of Linear Viscoelasticity* (Pergamon, London 1960).
[7] S. C. HUNTER, *Tentative Equations for the Propagation of Stress, Strain and Temperature Fields in Viscoelastic Solids*, J. Mech. Phys. Solids, *9*, 39–51 (1961).

Zusammenfassung

Der Artikel behandelt isotherme Verformungen eines linearviskoelastischen Stoffes im einachsigen Spannungszustand. Die Deformationsgeschichte des Materials für den Zeitabschnitt $(-\infty, 0)$ wird als bekannt angesehen. Ein Teil der mechanischen Arbeit, die am Material während dieses Zeitabschnitts geleistet wird, kann in rein mechanischer Weise dadurch zurückgewonnen werden, dass der Körper geeigneten weiteren Verformungen unterworfen wird. Der Artikel behandelt den Höchstbetrag, der auf diese Weise zurückgewonnen werden kann.

(Received: May 21, 1963.)

Flow of Rarefied Gas Over an Enclosed Rotating Disk[1])

By SHAO L. SOO, Dpt. of Mech. Engineering, University of Illinois, Urbana, Ill., USA, and ZUHAIR N. SARAFA, Dpt. of Mech. Engineering, University of Kansas, Lawrence, Kansas, USA

Notations

a outer radius of the disk
a_1, a_2, a_3, a_4, a_5 constants of integration defined by Equation (2.10)
b_1, b_2 constants of integration defined by Equation (3.8)
c_ϕ friction coefficient defined by the relation $c_\phi = \tau_s/(\frac{1}{2})\,\varrho_1\, r^2\,\omega^2$
c_p specific heat at constant pressure
$G(\eta)$ dimensionless function of the tangential velocity defined by the relation $V = R\,G(\eta)$
K dimensionless viscosity or thermal conductivity, μ/μ_1 or λ/λ_1
L mean free path
$\mathfrak{L}$ dimensionless mean free path defined by L/L_1
$\mathfrak{L}_s$ dimensionless mean free path defined by L_s/z_o
$(M)_1, (M)_r$ Mach numbers defined by $\omega\, L_1/\sqrt{\gamma\, \underset{\sim}{R}\, T_1}$, $\omega\, r/\sqrt{\gamma\, \underset{\sim}{R}\, T_1}$

[1]) A study supported by the National Science Foundation under grant No. G-9725. The experimental portion of this paper was performed by Z. N. SARAFA toward a thesis for partial fulfillment of the requirements of the Ph. D. Degree at the University of Illinois.

$N_1'(\eta)$ reduced radial velocity function given by $U - R\,N_1'(\eta)$
$(N_{Kn})_{z_0}$, $(N_{Kn})_d$ Knudsen numbers defined by L/z_0, L/d
$(N_{Pr})_1$ Prandtl number defined by $(c_p\,\mu_1)/\lambda_1$
$(N_{Re})_1$ Reynolds number $(\varrho_1\,\omega\,L_1^2)/\mu_1$
$(N_{Re})_r$ Reynolds number $(\varrho_1\,\omega\,r^2/\mu_1$
$(N_{Re})_0$ Reynolds number $(\varrho_1\,\omega\,z_0^2)/\mu_1$
p static pressure
Q reduced temperature function for heat exchange
$r,\ \theta,\ z$ cylindrical polar coordinates in the radial, azimuthal, and axial directions
$\underset{\sim}{R}$ gas constant in $p = \varrho\,\underset{\sim}{R}\,T$
$\tilde{R},\ Z$ dimensionless coordinates, r/L_1, z/L_1
S reduced temperature function for dissipation
S_w, S_s molecular speed ratios $r\,\omega/\sqrt{2\,\underset{\sim}{R}\,T_1}$, $v_s/\sqrt{2\,\underset{\sim}{R}\,T_1}$
T temperature
$u,\ v,\ w$ components of the velocity in the radial, tangential and axial directions
$U,\ V,\ W$ dimensionless velocity components $u/\omega\,L_1$, $v/\omega\,L_1$, $w/\omega\,L_1$
z_0 axial distance between disk and plate
α accommodation coefficient
β_1 dimensionless parameter defined by $\beta_1 = \sqrt{(N_{Re})_1/\sigma}$
β_0 dimensionless parameter defined by $\beta_0 = \sqrt{(N_{Re})_0/\sigma}$
γ ratio of specific heats
Γ dimensionless density given by ϱ/ϱ_1
ζ dimensionless axial coordinate given by z/z_0
η transformed dimensionless axial coordinate defined by $\beta_1\,\psi = -\,RN(\eta)$
θ dimensionless temperature T/T_1
$\varkappa$ constant equal to $75\,\pi/128$
λ thermal conductivity
μ viscosity
ϱ density
σ factor of proportionality defined by $(\mu/\mu_1) = \sigma(T/T_1)$
ψ dimensionless stream function
$\omega,\ \omega_c$ angular velocity of rotation of disk and fluid core respectively
Ω dimensionless angular velocity

Introduction

The present study extends from two earlier papers by Soo [1, 2][2]) to the case of motion of rarefied gas between a rotating disk and a parallel stationary plate at a finite distance away from the disk. The latter system is defined as an enclosed disk (Figure 1). Additional bibliographies are to be found in these earlier papers.

The present problem is significant from the point of view of performance of rotating elements in space (vacuum) environments and instances as the airlubricated bearing where the mean free path L of the fluid is not negligible when compared to the gap or other characteristic dimensions of the system.

[2]) Numbers in brackets refer to References, page 38.

An earlier study [1] showed that a rotating disk is a convenient system for studying slip and free molecule flow because the product of the characteristic Knudsen number N_{Kn} and the Mach number M_r, based on the radius of the disk, cancel out the radius r as a characteristic dimension. Only the pressure p, angular velocity ω and temperature T determine the range of $N_{Kn}\, M_r\, [= (L/r)\, (r\,\omega/\sqrt{\gamma\, \underset{\sim}{R}\, T}]$ or the regime of the flow phenomenon as viscous, slip, or free molecule flow; $\underset{\sim}{R}$ is the gas constant and γ is the ratio of specific heats. Since slip motion, when it occurs, is found at all radii, large magnitudes of slip motion can be measured accurately at a large radius of a rotating disk. Therefore, a rotating disk furnishes, in a sense, a magnified model of slip motion.

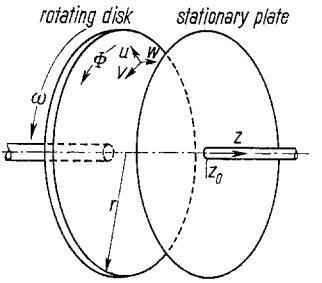

Figure 1

Coordinate system of an enclosed rotating disk.

As shown in the following, the enclosed rotating disk makes possible measurement in the slip and free molecule regime at both very small characteristic Reynolds numbers and Mach numbers. Thus, the effect of compressibility is negligible. This is not easily accomplished when an experiment is carried out with a flat-plate system [3].

It is also shown that continuous transition from slip to free molecule motion can be computed based on the Maxwell slip boundary conditions [4]. The experimental program makes possible a test of this boundary condition at near free-molecule flow states.

We use the experimental program to determine the effect of a finite disk diameter. Theoretical results cover the case of infinite disk and infinite plate. Experimental results show that the effect of a finite disk on the nature of slip motion is small.

1. Basic Formulation

Laminar boundary layer motion over an infinite rotating disk at a finite distance z_0 from a parallel infinite plate has the following order of magnitude of velocities [2, 5]:

$$U = 0\, [(N_{Re})_1\, R] \tag{1.1}$$

$$V = 0\, [R], \tag{1.2}$$

$$W = 0\, [(N_{Re})_1\, Z], \tag{1.3}$$

where U, V, and W are dimensionless radial, tangential and axial velocities:

$$U = \frac{u}{\omega\, L_1}, \qquad V = \frac{v}{\omega\, L_1}, \qquad W = \frac{w}{\omega\, L_1}, \tag{1.4}$$

where u, v, and w are the radial (coordinate r, measured from the axis of rotation), tangential (coordinate ϕ) and axial (coordinate z, measured from the surface of the rotating disk) velocities; L_1 is the reference mean free path of the fluid away from the wall [6].

$$L_1 = \frac{16}{5} \frac{\mu_1}{\varrho_1 \sqrt{2\pi \bar{R} T_1}}, \tag{1.5}$$

where ϱ_1, μ_1, T_1 are the density, the viscosity and the temperature at reference state [1]; ω is the angular velocity of rotation; the dimensionless coordinates R and Z are given by:

$$R = \frac{r}{L_1}, \quad Z = \frac{z}{L_1}. \tag{1.6}$$

$(N_{Re})_1$ is the characteristic Reynolds number given by:

$$(N_{Re})_1 = \frac{L_1^2 \omega \varrho_1}{\mu_1}. \tag{1.7}$$

For the range of states of the fluid under consideration, *i.e.* the fluid has very low density,

$$(N_{Re})_1 < 1. \tag{1.8}$$

Further, we consider cases, where

$$R > Z. \tag{1.9}$$

We thus deal with the case, where

$$V > U > W. \tag{1.10}$$

Following the above simplifications, the equations of continuity, momentum and energy take the form:

$$\frac{1}{R} \frac{\partial}{\partial R} (\Gamma R U) + \frac{\partial}{\partial Z} (\Gamma W) = 0, \tag{1.11}$$

$$-\frac{\Gamma V^2}{R} = \Gamma \Omega^2 R + (N_{Re})_1^{-1} \frac{\partial}{\partial Z} \left(K \frac{\partial U}{\partial Z} \right), \tag{1.12}$$

$$\frac{\partial}{\partial Z} \left(K \frac{\partial V}{\partial Z} \right) = 0, \tag{1.13}$$

$$\Gamma \left(U \frac{\partial \theta}{\partial R} + W \frac{\partial \theta}{\partial Z} \right) = (N_{Re})_1^{-1} (N_{Pr})_1^{-1} \frac{\partial}{\partial Z} \left(K \frac{\partial \theta}{\partial Z} \right), \tag{1.14}$$

where the radial pressure p gradient is given by [5, 7]:

$$-\frac{\partial p}{\partial r} = \varrho \omega_c^2 r, \tag{1.15}$$

where ϱ is the density of the fluid, ω_c is the angular velocity of the fluid core, and, in addition to the dimensionless variables explained earlier,

$$\theta = \frac{T}{T_1}, \quad \Gamma = \frac{\varrho}{\varrho_1}, \quad \Omega = \frac{\omega_c}{\omega}, \quad K = \frac{\mu}{\mu_1} = \frac{\lambda}{\lambda_1}, \quad N_{Pr} = \frac{c_p \mu}{\lambda} \tag{1.16}$$

λ and c_p being the thermal conductivity and specific heat at constant pressure of the

fluid; and, following CHAPMAN and RUBESIN [8]:

$$K\,\Gamma = \sigma \tag{1.17}$$

where σ is nearly a constant for a given range of temperature.

The Maxwell boundary conditions for slip flow are, at the disk ($z = 0$, $Z = 0$):

$$U_s = \mathcal{L}\left(\frac{\partial U}{\partial Z}\right)_s, \quad V_s - R = \mathcal{L}\left(\frac{\partial V}{\partial Z}\right)_s, \quad W_s = 0, \quad \theta_s - \theta_w = \varkappa\,\mathcal{L}\left(\frac{\partial \theta}{\partial Z}\right)_s, \tag{1.18}$$

where

$$\varkappa = \frac{75\,\pi}{128}, \quad \mathcal{L} = \frac{L}{L_1} \tag{1.19}$$

and subscript s refers to the conditions of the fluid at the wall, and w refers to the conditions at the wall; at the plate ($z = z_0$, $Z = Z_0$):

$$U_p = -\,\mathcal{L}\left(\frac{\partial U}{\partial Z}\right)_p, \quad V_p = -\,\mathcal{L}\left(\frac{\partial V}{\partial Z}\right)_p, \quad W_p = 0, \quad \theta_p - 1 = -\,\varkappa\,\mathcal{L}\left(\frac{\partial \theta}{\partial Z}\right)_p. \tag{1.20}$$

2. Flow Characteristics

The solution of Equations (1.11) to (1.14) subjecting to the above boundary conditions can be obtained by using a similar transformation as in Reference [1]. Introducing stream function ψ such that

$$\Gamma\,U = \frac{\partial \psi}{\partial Z}, \quad \Gamma\,W = -\,\frac{1}{R}\,\frac{\partial R\,\psi}{\partial R}, \tag{2.1}$$

and transforming the coordinates to R and η, such that

$$-\,R\,N(\eta) = \beta_1\,\psi\,, \tag{2.2}$$

where $\beta_1 = \sqrt{(N_{Re})_1/\sigma}$, and N is a function of η. Equations (1.12) and (1.13) now take the form:

$$N'' = -\,\Omega^2 - G^2, \tag{2.3}$$

$$G'' = 0 \tag{2.4}$$

as in Reference [2], and are independent of the energy equation,

$$U = R\,N'(\eta), \quad V = R\,G(\eta), \quad W = -\,\frac{1}{\beta_1}\,N(\eta) \tag{2.5}$$

and the boundary conditions are now:

$$\left.\begin{aligned} &N'(0) = -\,\beta_1\,N''(0), \quad 1 - G(0) = \beta_1\,G'(0), \\ &N'(\eta_0) = \beta_1\,N''(\eta_0), \quad G(\eta_0) = \beta_1\,G'(\eta_0), \quad N(0) = 0 = N(\eta_0), \end{aligned}\right\} \tag{2.6}$$

where, for given R,

$$\frac{z}{L_1} = Z = -\int_0^{\eta} \frac{d\eta}{\beta_1\,\Gamma} \tag{2.7}$$

and

$$\frac{z_0}{L_1} = Z_0 = -\int_0^{\eta_0} \frac{d\eta}{\beta_1 \Gamma} \tag{2.8}$$

Solution of Equations (2.3) and (2.4), subjecting to Equation (2.6), gives:

$$G = \frac{\eta}{2\beta_1 - \eta_0} + \frac{\beta_1 - \eta_0}{2\beta_1 - \eta_0}, \tag{2.9}$$

$$N = a_1 \eta + a_2 \eta^2 + a_3 \eta^3 + a_4 \eta^4 + a_5 \eta^5, \tag{2.10}$$

with

$$\left.\begin{aligned} a_1 &= \frac{-\beta_1 \eta_0^3 (5\beta_1 - \eta_0)}{10 (2\beta_1 - \eta_0)^2 (6\beta_1 - \eta_0)}, \\ a_2 &= \frac{\eta_0^3 (5\beta_1 - \eta_0)}{20 (2\beta_1 - \eta_0)^2 (6\beta_1 - \eta_0)}, \qquad a_3 = -\frac{\eta_0 (60\beta_1^2 - 50\beta_1 \eta_0 + 7\eta_0^2)}{60 (2\beta_1 - \eta_0)^2 (6\beta_1 - \eta_0)}, \\ a_4 &= -\frac{(\beta_1 - \eta_0)}{12 (2\beta_1 - \eta_0)}, \qquad a_5 = \frac{1}{60 (2\beta_1 - \eta_0)^2}. \end{aligned}\right\} \tag{2.11}$$

For the case of incompressible viscous motion, $\beta_1 \to 0$, $\eta_0 \to -1$, $\eta \to -z/z_0$,

$$G = 1 - \eta \tag{2.12}$$

and

$$a_1 = 0, \qquad a_2 = -\frac{1}{20}, \qquad a_3 = -\frac{7}{60}, \qquad a_4 = -\frac{1}{12}, \qquad a_5 = \frac{1}{60}, \tag{2.13}$$

as given in Reference [2]. Slip modifies the tangential, axial and radial velocities as shown in Figures 2 and 3; $\beta_1 \to \infty$ corresponds to free-molecule flow. Hence, in the present configuration, continuous transition from slip to free molecule flow can be accounted for.

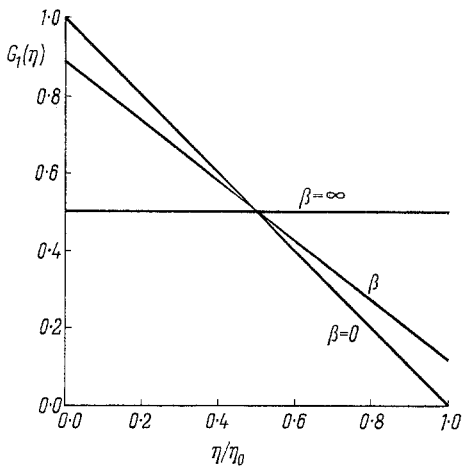

Figure 2
Tangential velocity profiles.

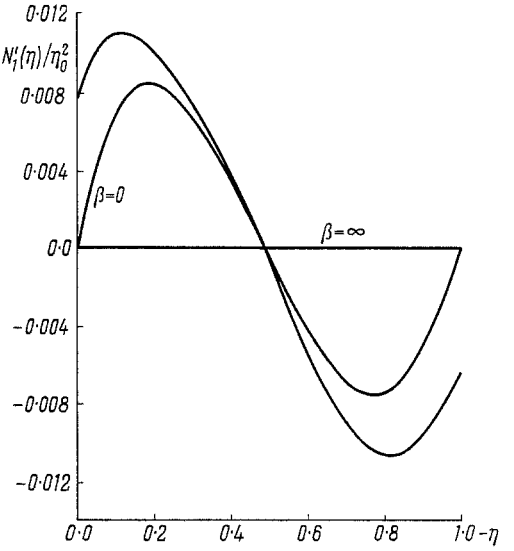

Figure 3
Radial velocity profile.

The pressure distribution remains according to:

$$\beta_1 \to 0, \quad G\left(\frac{\eta_0}{2}\right) = \frac{1}{2}, \quad \Omega^2 = \frac{1}{4}; \quad \beta_1 \to \infty, \quad G = \frac{1}{2}, \quad \Omega^2 = \frac{1}{4}.$$

The local rates of shear at the disk surface are

$$\left.\frac{\partial u}{\partial z}\right]_0 = -\omega\,\beta_1\,R\,\Gamma_w\,N''(0) = -\omega^{3/2}\sqrt{\frac{\varrho_1}{\mu_1}}\,\frac{T_1}{T_w}\,r\,N''(0), \tag{2.14}$$

where

$$N''(0) = 2\,a_2 = \frac{\eta_0^3\,(5\,\beta_1 - \eta_0)}{10\,(2\,\beta_1 - \eta_0)^2\,(6\,\beta_1 - \eta_0)} \tag{2.15}$$

and

$$\left.\frac{\partial v}{\partial z}\right]_0 = -\omega\,\beta_1\,R\,\Gamma_w\,G'(0) = -\omega^{3/2}\sqrt{\frac{\varrho_1}{\mu_1}}\,\frac{T_1}{T_w}\,r\,G'(0), \tag{2.16}$$

where

$$G'(0) = \frac{1}{2\,\beta_1 - \eta_0} \tag{2.17}$$

3. Temperature Distribution

It remains to transform η back to the physical coordinate by solving the energy equation. With the solution given by:

$$\theta = 2\,(\gamma - 1)\,M_1^2\,R^2\,S(\eta) + (\theta_s - \theta_p)\,Q(\eta) + \theta_p, \tag{3.1}$$

where θ_s is the dimensionless temperature of the gas at the disk surface, θ_p is that at the stationary plate, and $M_1 = \omega\,L_1/\sqrt{\gamma\,\underset{\sim}{R}\,T_1}$ is a characteristic Mach number. The

energy equation is now separable:

$$\frac{1}{N_{Pr}} Q'' + 2 N Q' = 0 , \tag{3.2}$$

$$\frac{1}{N_{Pr}} S'' + 2 N S' - 2 N' S = - (N''^2 + G'^2), \tag{3.3}$$

which are identical to the forms arrived at by MILLSAPS and POHLHAUSEN; and the solution was derived in Reference [9].

We can consider the following cases of boundary condition:

Case I. Constant temperature system, at the solid surfaces, $T(0) = T_w$, $T(z_0) = T_1$.

Case II. Constant disk temperature, plate insulated; at the solid surfaces, $T(0) = T_w$, $\partial T/\partial z]_{z_0} = 0$.

Case III. Case I with negligible convection (rarefied gas).

Case I

The slip boundary conditions of the fluid of Case I are:

$$\theta_s - \theta_w = - \varkappa \beta_1 \frac{\partial \theta}{\partial \eta}\Big]_0 , \tag{3.4}$$

$$\theta_p - 1 = \varkappa \beta_1 \frac{\partial \theta}{\partial \eta}\Big]_{\eta_0} . \tag{3.5}$$

The accommodation coefficients, α_s and α_p, are

$$\alpha_s = \frac{\theta_s - \theta_p}{\theta_w - \theta_p} , \qquad \alpha_p = \frac{\theta_s - \theta_p}{\theta_s - 1} . \tag{3.6}$$

The boundary condition, when separated, becomes:

$$\left.\begin{aligned} Q(0) + \varkappa \beta_1 Q'(0) = \frac{1}{\alpha_s} , \qquad S(0) = - \varkappa \beta_1 S'(0), \\ Q_1(\eta_0) - \varkappa \beta_1 Q'(\eta_0) = 1 - \frac{1}{\alpha_p} , \qquad S(\eta_0) = \varkappa \beta_1 S'(\eta_0). \end{aligned}\right\} \tag{3.7}$$

The equation of Q_1 is readily integrated:

$$Q_1 = b_1 \int_0^\eta \exp\left[- 2 N_{Pr} \int_0^\eta N \, d\eta \right] d\eta + b_2 , \tag{3.8}$$

for $\alpha_s = \alpha_p = \alpha$,

$$b_1 = \frac{1 - 2/\alpha}{I - \beta_1 \varkappa (1 + I')} , \tag{3.9}$$

$$b_2 = \frac{1}{\alpha} - \frac{\varkappa \beta_1 (1 - 2/\alpha)}{I - \beta_1 \varkappa (1 + I')} , \tag{3.10}$$

where

$$I = \int_0^{\eta_0} \exp\left[- 2 N_{Pr} \int_0^\eta N \, d\eta \right] d\eta , \tag{3.11}$$

$$I' = \exp\left[- 2 N_{Pr} \int_0^\eta N \, d\eta \right] . \tag{3.12}$$

When there is no slip, $b_2 = 0$, $b_1 = -1/I$, as in Reference [9]. For complete slip, $\beta_1 \to \infty$, gives $b_1 = 0$, $b_2 = 1/2$ ($I' = 1$, $I = \eta_0$). The dissipation function $S(\eta)$ can be calculated in the same manner as in Reference [9]. The trend of Q and S are as shown in Figure 4, for a given Prandtl number.

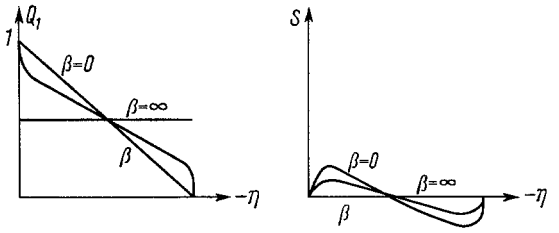

Figure 4
Trend of temperature distribution for constant wall temperatures.

Case II

The boundary condition at the plate is now:

$$\frac{\partial \theta}{\partial \eta}\Big]_{\eta_0} = 0 \tag{3.13}$$

which gives

$$S'(\eta_0) = 0\,, \qquad Q'(\eta_0) = 0\,, \tag{3.14}$$

$$\text{or, } b_1 = 0,\ b_2 = 1/\alpha, \text{ and } \theta = 2(\gamma - 1) M_1^2 R^2 S(\eta) + \theta_w \tag{3.15}$$

and the contribution is entirely due to dissipation. The trend, following solution as in Reference [9], is shown in Figure 5.

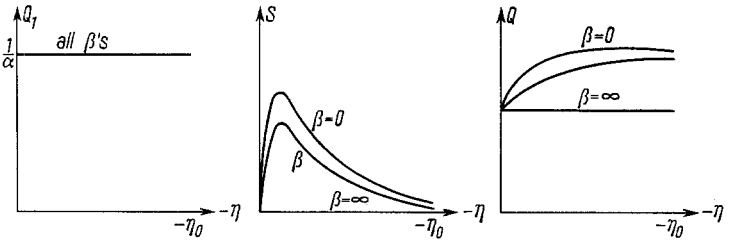

Figure 5
Temperature distribution for insulated plate.

Case III

This case is closely related to our experimental program where the convection effect is small, or, Equation (3.2) is reduced to:

$$\frac{d^2\theta}{d\eta^2} = 0\,. \tag{3.16}$$

Its solution with the given boundary conditions is:

$$\theta = \frac{\varkappa \beta_1 (\theta_w + 1) - \theta_w \eta_0}{2\varkappa \beta_1 - \eta_0} + \frac{(\theta_w - 1)\eta}{2\varkappa \beta_1 - \eta_0}\,. \tag{3.17}$$

For motion without slip, $\beta_1 \to 0$,

$$\theta = \theta_w - \frac{(\theta_w - 1)\eta}{\eta_0} \tag{3.18}$$

and for the case of free molecule flow, $\beta_1 \to \infty$,

$$\theta = \frac{\theta_w + 1}{2}. \tag{3.19}$$

The trend is plotted in Figure 6.

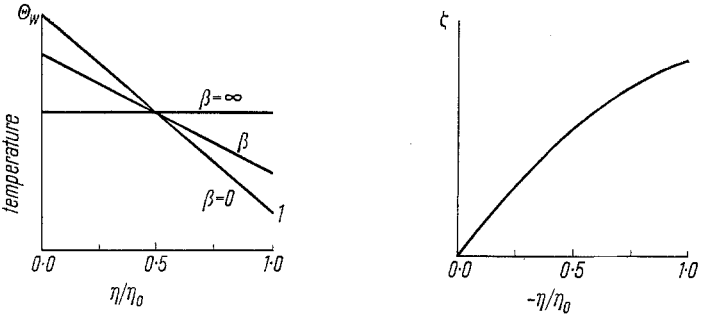

Figure 6
Temperature distribution and relation between η and ζ.

The physical coordinate z can now be determined:

$$\left.\begin{aligned} \zeta = \frac{z}{z_0} &= -\frac{1}{\beta_0}\int_0^\eta \theta\, d\eta \\ &= -\frac{1}{\beta_0}\left[\frac{\varkappa\beta_1(\theta_w+1) - \theta_w\eta_0}{2\varkappa\beta_1 - \eta_0} + \frac{(\theta_w-1)\eta^2}{2(2\varkappa\beta_1 - \eta_0)}\right], \end{aligned}\right\} \tag{3.20}$$

where $\beta_0 = \beta_1 z_0/L_1$. Equation (3.20) shows that the relation between z and η is parabolic. For $\beta_1 \to 0$,

$$\zeta = \frac{z}{z_0} = -\frac{1}{\beta_0}\left[\theta_w\eta - \frac{(\theta_w - 1)}{2\eta_0}\eta^2\right] \tag{3.21}$$

at the plate, $\eta = \eta_0$,

$$\zeta = \frac{z}{z_0} = -\frac{1}{\beta_0}\left(\frac{\theta_w + 1}{2}\right)\eta_0. \tag{3.22}$$

For a constant temperature system as in our experimental study,

$$\zeta = \frac{z}{z_0} = -\frac{\eta}{\beta_0}, \tag{3.23}$$

giving a linear relation between η and z with proportionality based on:

$$(N_{Re})_0 = \frac{z_0^2\,\omega\,\varrho_1}{\mu_1}, \tag{3.24}$$

thus reverting to the case of incompressible fluid. Our experiments approximate this condition very closely.

4. Friction Coefficient and Slip Factor

The local tangential friction coefficient c_ϕ can be calculated from:

$$c_\phi = \frac{\mu\,(\partial v/\partial z)_0}{(1/2)\,\varrho\, r^2\,\omega^2}\,. \tag{4.1}$$

From the above results, for a constant temperature system, with the Mach number based on radius $M_r = \omega\, r/\sqrt{\gamma\, \underset{\sim}{R}\, T_1}$:

$$c_\phi\, M_r = \frac{M_r^2}{(N_{Re})_r}\left(\frac{r}{z_0}\right)\frac{2}{M_r\,[2\,(L_1/z_0)+1]}\,, \tag{4.2}$$

where $(N_{Re})_r$ is given by:

$$(N_{Re})_r = \frac{\varrho_1\, r^2 \omega}{\mu_1} \tag{4.3}$$

and reduces to

$$c_\phi\, M_r = \frac{5}{16}\,\frac{2\,\pi}{\gamma} \tag{4.4}$$

for free molecule flow; and to

$$c_\phi\, M_r = \frac{M_r^2}{(N_{Re})_r}\left(\frac{r}{z_0}\right)\frac{2}{M_r} \tag{4.5}$$

for viscous flow. At higher $(N_{Re})_{z_0}$, we have

$$c_\phi\, M_r = 0{\cdot}856\left[\frac{M_r^2}{(N_{Re})_r}\right]^{1/2} \tag{4.6}$$

for laminar boundary layer motion as obtained by SCHULTZ-GRUNOW [16].

The above is to be compared to

$$c_\phi\, M_r = \frac{2}{\sqrt{3\,\pi\,\gamma}} \tag{4.7}$$

for free molecule flow over a free disk; and

$$c_\phi\, M_r = 0{\cdot}61\,\frac{\sqrt{5}}{2}\left(\frac{2\,\pi}{\gamma}\right)^{1/4}\frac{\sigma_w}{\sqrt{\sigma}}\left[\frac{M_r^2}{(N_{Re})_0}\right]^{1/2} \tag{4.8}$$

for the laminar flow range [1, 10].

The slip factor can be obtained from:

$$V_s - R = \mathcal{L}\left(\frac{\partial V}{\partial Z}\right)_s, \tag{4.9}$$

where, in terms of the molecular speed ratio [4]:

$$S_s = \frac{v_s}{\sqrt{2\,\underset{\sim}{R}\,T_1}} \qquad S_w = \frac{r\,\omega}{\sqrt{2\,\underset{\sim}{R}\,T_1}} \tag{4.10}$$

gives:

$$S_s - S_w = \mathcal{L}_s\left(\frac{\partial S}{\partial \zeta}\right)_s, \tag{4.11}$$

where $\zeta = z/z_0$, and $\mathcal{L}_s = L_s/z_0$. As a test of the Maxwell boundary condition for slip flow, we may take the characteristic group as our reference:

$$S_w\,\mathcal{L}_s = \sqrt{\gamma}\,\frac{r}{z_0}\left[\frac{M_r^2}{(N_{Re})_r}\right] \tag{4.12}$$

and measurement of slip factor $\mathcal{L}_s$ will provide a test for the Maxwell boundary condition for slip flow.

5. Experimental Equipment and Instrumentation

For the experimental program a test facility was designed and constructed in which a disk is driven at speeds of 1000 rpm to 20000 rpm inside a vacuum chamber (2′ × 5-1/2′ inside dimension) with provisions for measuring pressure and temperature distributions over the entire surface of the disk.

Pumpdown (to 1μ Hg) of the vacuum chamber consists of a 6″ elbow welded to the chamber on one side, and connected to the diffusion pump with an 0-ring seal. A 2″ 'Veeco' vacuum valve is placed between the diffusion pump and the mechanical pump. The disk and probe mechanism assemblies slide into the chamber on two channels welded inside the chamber in such a way that the disk center is the same as that of the chamber.

Figure 7 shows a detailed drawing of the disk used in this experiment. The 12″ diameter disk was constructed from 7075-TG ALCOA aluminum alloy. The face of the disk was machined and ground to a very smooth finish (variation across the diameter was less than 0·001″). The disk was mounted directly on the motor shaft using an 'American Standard force fit, class FN_1'. The disk is driven by a special three-phase, 400 cycle induction motor designed for operation in a vacuum. The motor input is

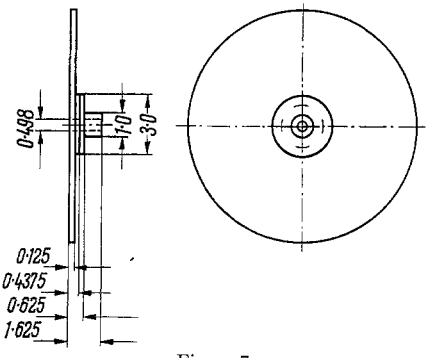

Figure 7
Disk design details.

delivered from a 60- to 400-cycle frequency converter, which in turn is operated from a variable transformer with 110 volt AC input. This disk drive unit is capable of variable speeds ranging from 1000 rpm to 20000 rpm. For speed counting, a small magnet is mounted into an 0·25″ hole drilled in a stainless steel shaft. The stainless steel shaft, which is 1″ long and 0·5″ in diameter, is screwed into the motor shaft. A small earphone coil is mounted directly underneath the magnet. When the disk rotates, a signal is produced every time the magnet completes a full revolution over the coil. The signal is magnified by an amplifier, then fed into an electronic counter for speed indication.

A probe holder designed for both axial and radial traverse is mounted on the frame of the rotating disk system. Traverse of the probe holder is made through two shafts

extended to the outside of the vacuum chamber through two vacuum seals [11]. These vacuum tight seals allow rotation and translation of a half-inch shaft without affecting the pressure in the chamber.

Measurement of the chamber pressure and the calibration of the Pirani gauge were made with a mercury McCleod gauge. The McCleod gauge is provided with direct reading scales so that no computation is needed. Both chamber pressure measurement and the velocity head measurement were made with Pirani gauges. For the measurement of the velocity head in vacuum, a differential Pirani gauge was designed [12]. The calibration of the differential Pirani gauge for air and argon are shown in Figures 8 and 9. The pressure probes are shown in Figure 10. The time con-

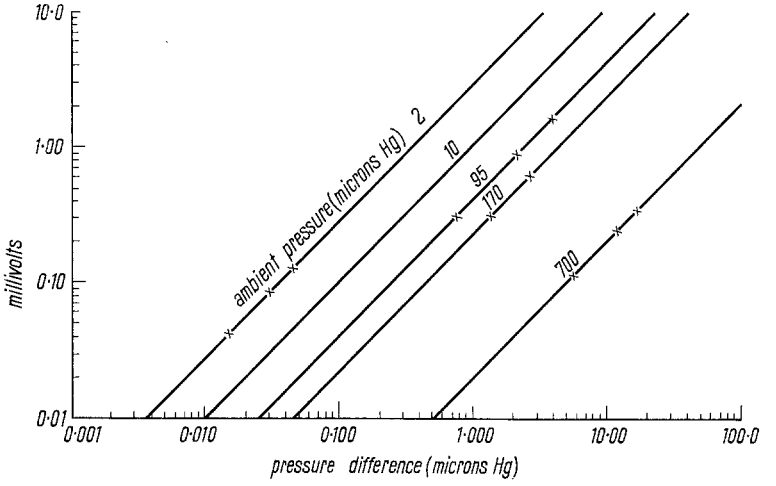

Figure 8
Calibration curves for air.

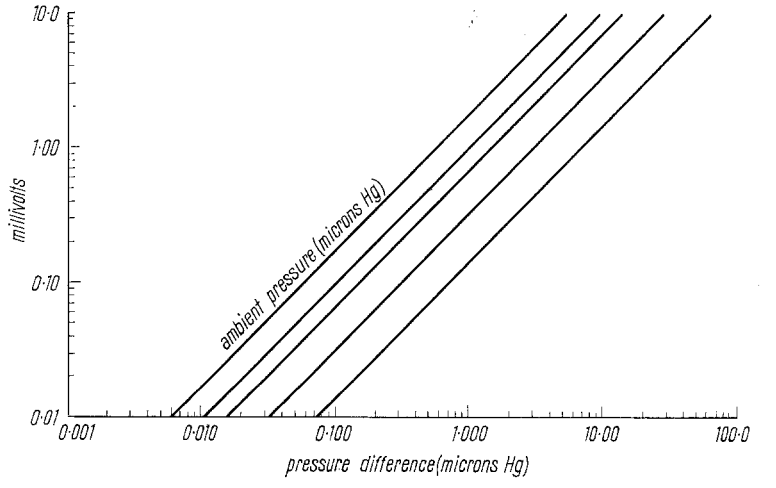

Figure 9
Calibration curves for argon.

stant [13] for measurements down to 2μ Hg pressure is less than 10 minutes. The variation of static pressure due to rotation at low densities amounts to less than 0·01 μ per μ Hg of pressure, which is below the sensitivity of the gauge system.

For the determination of the actual velocity head, the calibration follows HARRIS and PATTERSON [14]. This calibration, when compared to the earlier method of CHAMBRE and SCHAAF [15], is shown in Figure 11. All probes were constructed of

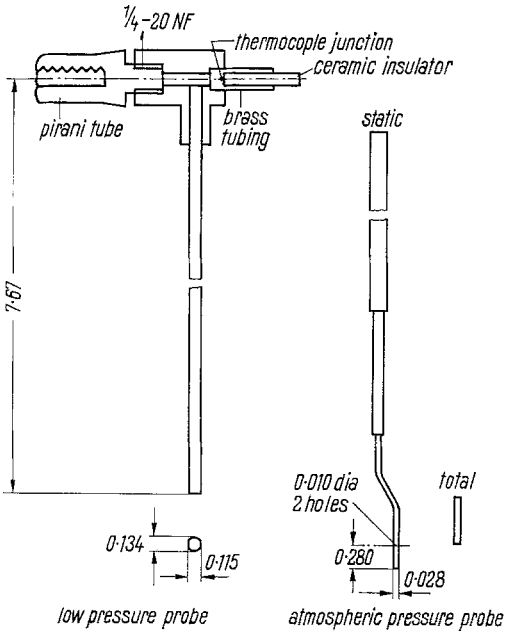

Figure 10
Pressure probes used in the experiments.

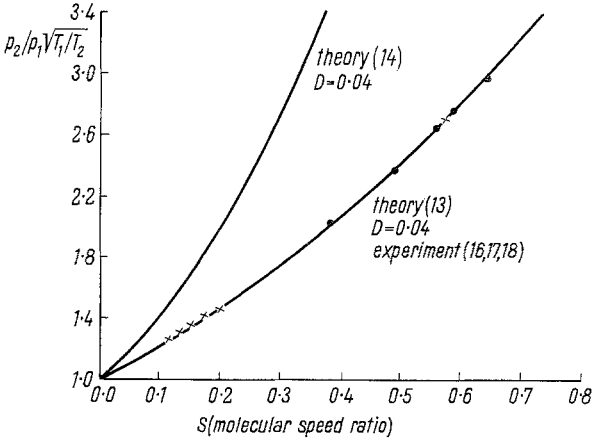

Figure 11
Comparison between theory and experiment of long tube impact in free molecule flow.

sections of stainless steel tubing. Their sizes were chosen as a compromise between the requirements of being small enough to minimize flow disturbance, and large enough to improve the time response – the latter being a special problem for making measurements in rarefied gas.

6. Experimental Procedure and Results

In the beginning, measurements were made in the continuum regime; the results compare favorably to earlier published results [20]. Later measurements of difference between the impact pressure in the tangential direction due to rotation of the disk and static pressure were recorded using the differential Pirani gauge. The measurement technique described in Reference [12] was used. The closest setting of the impact probe is 0·064″ from the disk surface. By means of the vernier controls outside the chamber the probe was traversed across the entire gap between the rotating disk and the stationary plate. Data were recorded at increments of 0·180″ to 0·0945″ across the gap for gaps of 1″ and 1/2″ respectively. In addition to impact pressure measurements, temperatures were also recorded using a copper-constantan thermocouple. The thermocouple was mounted at the end of the impact probe.

The measured stagnation temperatures were nearly the same as the ambient temperature with a maximum difference of 2° F, following the values predicted by [4]:

$$\frac{T_2}{T_1} = 1 + \frac{2}{5} S^2,$$

whereas the maximum value of S in our experiments is 0·35. Hence, the relation as derived for the iso-thermal system in the above is accurate for the present system. From the ratio of the impact to static pressure, the molecular speed ratio S is determined from Figure 12, which is a plot based on Reference [14] for diameter to length ratio of 0·015, as in our experiments.

For the determination of the slope $\partial S/\partial \zeta$ and slip $S_s - S_w$ from the experimental data, a fourth degree polynomial was used, and the coefficients of the polynomial in

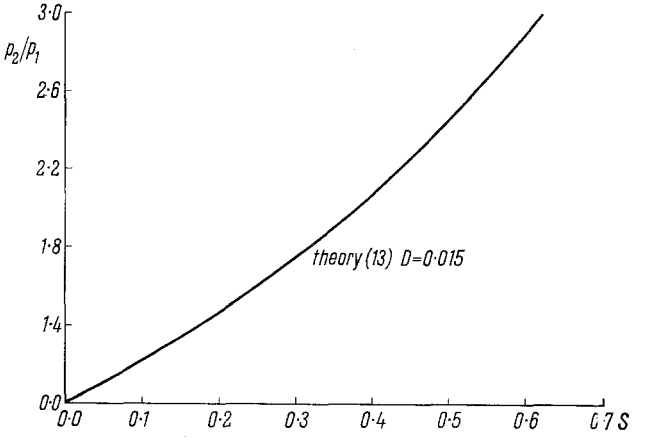

Figure 12
Molecular speed ratio versus pressure ratio.

terms of the gap were determined by solving a set of five simultaneous equations for each run. c_ϕ is given by Equation (4.1) and the slip factor $\mathcal{L}_s^c$ is given by Equation (4.11).

The results of the experiments are presented in Figure 13, which is plotted in comparison to Equation (4.12); Figure 14 is a comparison to the relation for semi-infinite mediums [1]. Figures 15 and 16 are two typical plots showing the range of the experiment from slip and free molecule flow.

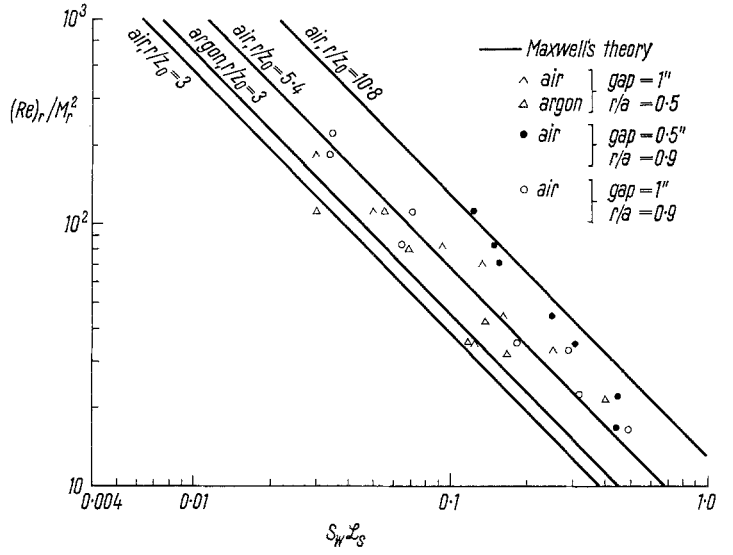

Figure 13
Slip factor.

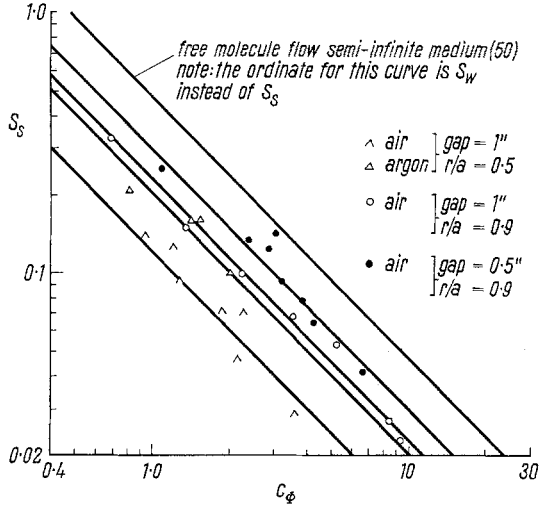

Figure 14
Friction coefficient.

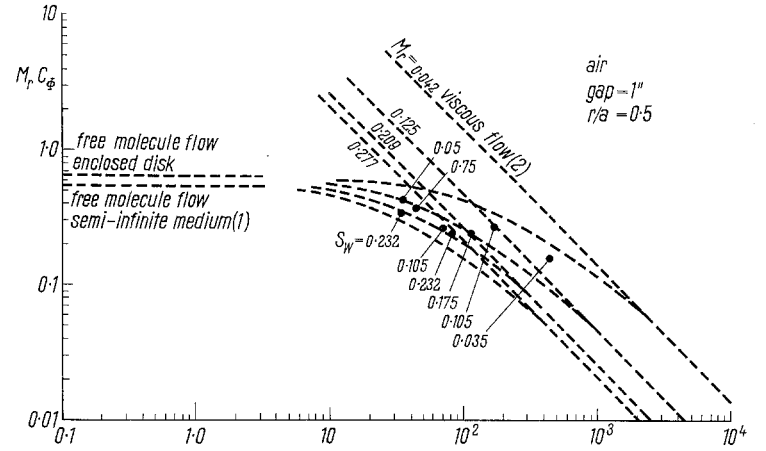

Figure 15

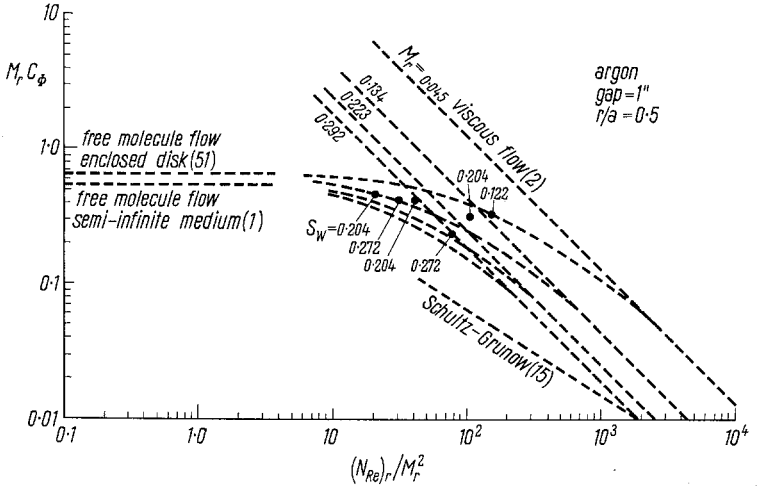

Figure 16

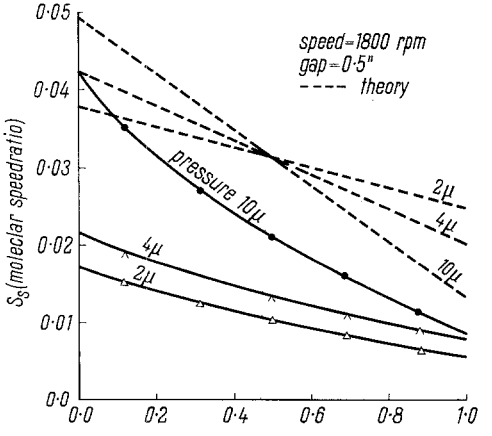

Figure 17

Tangential velocity profiles (comparison of theoretical and experimental curves showing finite disk effect).

These results show that in spite of the inherent difference between a finite disk from the infinite system used in the theoretical analysis [5], the validity of the theoretical model is demonstrated. A typical comparison is shown in Figure 17.

7. Discussion and Conclusions

From comparison of our theoretical and experimental results, it is shown that, with the rotating disk, transition from viscous to free molecule flow can be studied without involving the compressibility effect. Our experiments covered a wide range in slip motion. As was suggested earlier [1], the rotating disk furnishes a magnified model of slip motion. Even at moderate speeds and pressures we can obtain slip motion over the whole disk of 12″ diameter. The friction coefficient is shown to vary directly with radius and with the molecular weight of the gas and inversely with the gap. Transition from continuum to free molecule flow occurs through boundary layer motion [16], viscous motion, slip motion, and then free molecule motion.

REFERENCES

[1] S. L. Soo, *Transport Processes Involving a Moving Rotating Disk in a Low Density Gas*, Trans. ASME, J. of Basic Eng. *83* (3) (1961), 423.

[2] S. L. Soo, *Laminar Flow Over an Enclosed Rotating Disk*, Trans. ASME, J. of Basic Eng. *80* (2) (1958), 287.

[3] S. A. SCHAAF and P. L. CHAMBRE, *Flow of Rarefied Gases*, Princeton Aeronautical Paper Backs *8* (Princeton University Press 1961).

[4] G. N. PATTERSON, *Molecular Flow of Gases* (John Wiley and Sons, Inc., New York 1956).

[5] S. L. Soo and Z. N. SARAFA, *Fluid Motion Between two Coaxial Rotating Disks*, Univ. of Illinois, Mech. Eng. Dept. ME TN-9725-2, July 1960.

[6] H. S. TSIEN, *Superaerodynamics, Mechanics of Rarefied Gases*, J. of Aero. Sci., December 1946, 653.

[7] J. W. DAILY and R. C. NECE, *Roughness and Chamber Dimension Effects on Induced Flow and Frictional Resistance of Enclosed Rotating Disks*, MIT Hydrodynamics Lab. Tech. Rept. *27* (1958).

[8] D. R. CHAPMAN and M. W. RUBESIN, *Temperature and Velocity Profiles in the Compressible Laminar Boundary Layer with Arbitrary Distribution of Surface Temperature*, J. of Aero. Sci. *16* (1949), 547.

[9] K. MILLSAPS and K. POHLHAUSEN, *Heat Transfer by Laminar Flow from a Rotating Plate*, J. of Aero. Sci. *19* (1952), 120.

[10] T. VON KÁRMÁN, *Über laminare und turbulente Reibung*, Z. angew. Math. Mech. *1* (4) (1921), 224.

[11] R. R. WILSON, *Vacuum Seal*, Rev. of Sci. Inst. *12* (1941), 91.

[12] Z. N. SARAFA and S. L. SOO, *A Differential Pirani Gauge for Measuring Dynamic Pressure in a Rarefied Gas*, Rev. of Sci. Inst. *33* (10) (1962), 1077.

[13] S. A. SCHAAF and R. R. CYR, *Time Constants for Vacuum Gauge Systems*, J. of Appl. Phys. 20 (1949).

[14] E. L. HARRIS and G. N. PATTERSON, *Properties of Impact Pressure Probes in Free Molecule Flow*, Univ. of Toronto, Inst. of Aerophysics Rept. *52* (1958).

[15] P. L. CHAMBRE and S. A. SCHAAF, *The Theory of Impact Tube at Low Pressure*, J. of Aero. Sci. *15* (1948), 735.

[16] F. SCHULTZ-GRUNOW, *Der Reibungswiderstand rotierender Scheiben in Gehäusen*, Z. angew. Math. Mech. *15* (1935), 191.

[17] K. R. ENKENHUS, *Pressure Probes at Very Low Density*, Univ. of Toronto, Inst. of Aerophysics Rept. *43* (1957).

[18] E. L. HARRIS, *Investigation of Free Molecule and Transition Flows Near the Leading Edge of a Flat Plate*, Univ. of Toronto, Inst. of Aerophysics Rept. *53* (1958).

[19] E. P. MUNTZ, *Pressure Measurements in Free Molecule Flow with a Rotating Arm Apparatus*, Univ. of Toronto, Inst. of Aerophysics TN *22* (1958).

[20] S. GOLDSTEIN, *Modern Developments in Fluid Dynamics* (Clarendon Press, Oxford 1952).

Zusammenfassung

Es wird gezeigt, dass der Übergang von der Kontinuumsströmung zur «Gleitströmung» (slip-flow) an einer rotierenden Scheibe durch ihren Abstand von der ruhenden Wand, die Drehgeschwindigkeit und den Gasdruck bestimmt wird. Messungen zeigen, dass die Maxwellsche Grenzbedingung fast bis zur Molekularströmung herab erfüllt bleibt. Trotz der Unterschiede zwischen der theoretischen (unendlich ausgedehnten) und der wirklichen Scheibe werden die Reibungskoeffizienten für beide Fälle sehr ähnlich.

(Received: May 13, 1963.)

The Stability of Dissipative Couette Flow between Rotating Cylinders in the Presence of an Axial Magnetic Field

By ULRICH H. KURZWEG, United Aircraft Corporation, Research Laboratories, East Hartford, Conn., USA

1. Introduction

The effect of an axial magnetic field on the stability of Couette flow between concentric rotating cylinders has been examined by CHANDRASEKHAR [1][1]) for the case of a weakly conducting viscous fluid bounded by infinitely conducting, co-rotating cylinders. It was found that the magnetic field has a stabilizing influence, with the degree of stabilization being a function of the Hartmann number. NIBLETT [2] has re-examined this problem, using the more realistic assumption that the cylinders are insulators. His calculated values for the Taylor number at the onset of instability have recently been verified experimentally by DONNELLY and OZIMA [3].

In the present paper we extend Niblett's analysis to the case where the cylinders have an arbitrary rotation ratio. We will give an explicit evaluation for the critical Taylor and wave number as a function of the Hartmann number for all rotation ratios $| m | \leq 1$, where $m = \Omega_2/\Omega_1$ with Ω_1 and Ω_2 denoting the angular velocity of the inner and the outer cylinder, respectively. In addition, asymptotic formulas relating the Taylor and wave number to the magnitude of the magnetic field for very large Hartmann number, are obtained. Preliminary results of this investigation have been

[1]) Numbers in brackets refer to References, page 45.